Solving Microstrip Discontinuities by the Measured Equation of Invariance

Mark D. Prouty, *Member, IEEE,* Kenneth K. Mei, *Fellow, IEEE,* Steven E. Schwarz, *Fellow, IEEE,* Rafael Pous, *Member, IEEE,* and Yau-wu Liu

***Abstract*— The measured equation of invariance (MEI) is a newly developed computational method which allows finite-difference (FD) or finite-element (FE) mesh to be terminated very closely to objects of interest [1]. In this paper, the authors show how the MEI method may be applied to microstrip antennas and discontinuity problems. The authors demonstrate its use in general full-wave three-dimensional (3-D) microstrip problems, and give results for open-ended microstrip lines and microstrip bends. Sufficient details are included so that a well-versed reader may reproduce the authors' results with much less effort.**

I. Introduction

THE MEASURED equation of invariance (MEI) method is a newly developed computation technique, which allows finite-difference (FD) or finite-element (FE) meshes to be terminated very closely to the objects of interest [1]. Since its debut in 1992 [2], the method has been tested, criticized, or improved by numerous computer electromagnetists [3]–[14]. The remarkable feature of this method is its capability to truncate the mesh almost on to the object surface and still leave the sparsity of the FD/FE equations intact. In earlier work, the authors applied this method to two-dimensional (2-D) scattering from general object shapes and three-dimensional (3-D) scattering from sheet scatterers [1], to quasi-static microstrip structures [14], and to discontinuities in suspended striplines [15], [16].

The purpose of this paper is to demonstrate that the MEI method may be applied to microstrip structures. Since this is the first time the MEI is being applied to a complex 3-D problem, and a new FD mesh strategy is used on the vector and scalar potentials, the computer code is developed in a conservative way so as to minimize computational uncertainties, which might contribute to the failure of the computation. For example, no attempt was made to speed up the Sommerfeld's integrals by approximations. Thus, the efficiency of the MEI method as compared to other methods is not addressed. However, the lean mesh coverage and the sparsity of the matrix of the MEI method is a feature of special interest to computational electromagnetics. It is demonstrated that the MEI gives similar results as the method of moments (MoM) for infinite microstrips, open-ended microstrip lines, and microstrip bends.

Manuscript received June 10, 1995; revised February 28, 1997. This work was supported by USAF/Rome Laboratory under Contract F30602-94-1-0008, by the U.S. Army Research Office under Contract DAAL-03-90-G-0064, and by the City University of Hong Kong, Strategic Research Grant, 700-412.

M. D. Prouty was with the Department of Electrical Engingeering and Computer Sciences, University of California, Berkeley, Berkeley, CA 94720 USA. He is now with Geometric, Inc., Sunnyvale, CA 94086 USA.

K. K. Mei and Y. Liu were with the Department of Electrical Engingeering and Computer Sciences, University of California, Berkeley, Berkeley, CA 94720 USA. They are now with the Department of Electronic Engineering, City University of Hong Kong, Kowloon.

S. E. Schwarz is with the Department of Electrical Engingeering and Computer Sciences, University of California at Berkeley, Berkeley, CA 94720 USA.

R. Pous was with the Department of Electrical Engingeering and Computer Sciences, University of California, Berkeley, Berkeley, CA 94720 USA. He is now with University Politecnica de Catalunya, 08034 Barcelona, Spain.

Publisher Item Identifier S 0018-9480(97)03909-4.

II. Finite-Difference Formulation

The geometry of this investigation has been limited to planar metal strips on top of a flat grounded dielectric substrate. The meshes are rectangular in shape. Due to the planar metal configuration, the currents will be limited to the xz-plane, and the normal of the substrate is in the y-direction. The most convenient formulation of the Maxwell's equations for such a structure is to use the vector and scalar potentials

$$\bar{B} = \nabla \times \bar{A} \tag{1}$$

$$\bar{E} = -j\omega\bar{A} - \nabla\Phi \tag{2}$$

where

$$\nabla \cdot \bar{A} = -j\omega\mu\varepsilon\Phi \quad \text{(Lorenz gauge)} \tag{3}$$

$$(\nabla^2 + k^2)\bar{A} = -\mu\bar{J} \tag{4}$$

$$(\nabla^2 + k^2)\Phi = -\rho/\varepsilon \tag{5}$$

and

$$\nabla \cdot \bar{J} = -j\omega\rho. \tag{6}$$

The boundary conditions on the interface are

$$\hat{n} \times (\bar{H}_1 - \bar{H}_2) = J_s \tag{7}$$

and

$$\hat{n} \times (\bar{E}_1 - \bar{E}_2) = 0 \tag{8}$$

where $\hat{n}$ is the normal $(\hat{y})$ of the surface, and the subscripts represent the two sides of the interface. $J_s = 0$ when the node is not on the metal strip. J_s is an unknown when the node is on the metal, where (7) should be dropped and (8) should be replaced by

$$\left.\begin{aligned} \hat{n} \times \bar{E}_1 = 0 \\ \hat{n} \times \bar{E}_2 = 0 \end{aligned}\right\}. \tag{9}$$

Even though the current in this problem is in the xz-plane only, because of the presence of the dielectric substrate, the

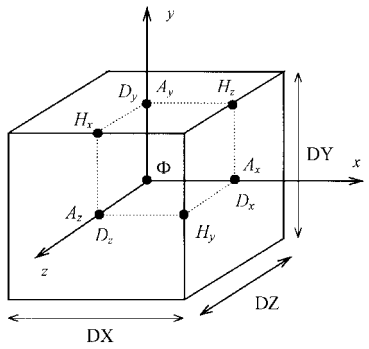

Fig. 1. Unit cell for the staggered mesh.

vector potential also contains a y-component. The solution of the Maxwell's equation is now reduced to that of solving the three scalar wave equations

$$(\nabla^2 + k^2)A_i = 0 \tag{10}$$

where $i = x$, y, or z. The equations are decoupled except at the interface. The FD equation of (10) is well known, but the key to a successful development of the FD equation is the node assignment for each vector potential component. The proper way to discretize the components of A is to stagger the locations at which the different components are calculated. Like Yee's lattice in time domain [17], such a node distribution provides a staggered node distribution for the components of the electric and magnetic field. A unit cell of the staggered mesh is shown in Fig. 1. For convenience, the superscripts of the vector potential are integers representing the discretization size DX, DY, DZ in the x-, y-, and z-directions respectively. The relations between the superscript and the real coordinate locations of the nodes are

$$\overline{A}^{(i,y,k)} = \begin{Bmatrix} A_x[(i+\frac{1}{2})DX, j\cdot DY, k\cdot DZ] \\ A_y[i\cdot DX, (j+\frac{1}{2})DY, k\cdot DZ] \\ A_z[i\cdot DX, j\cdot DY, (k+\frac{1}{2})DZ] \end{Bmatrix}. \tag{11}$$

A. Interior Equations in Uniform Medium

Based on the previously described node locations of the vector potential components, the FD equations of A_i from the standard central difference formulas can be obtained. A typical equation for A_x is

$$\begin{aligned} &DZ\cdot DY\left[\frac{2}{DX^2}+\frac{2}{DY^2}+\frac{2}{DZ^2}-k^2\right]A_x^{(i,j,k)} - DZDY \\ &\cdot\left\{\frac{A_x^{(i+1,j,k)}+A_x^{(i-1,j,k)}}{(DX)^2}+\frac{A_x^{(i,j+1,k)}+A_x^{(i,j-1,k)}}{(DY)^2}\right. \\ &\left.+\frac{A_x^{(i,j,k+1)}+A_x^{(i,j,k-1)}}{(DZ)^2}\right\} = \mu I_x^{(i,j,k)}. \end{aligned} \tag{12}$$

Note that the location of I_x and E_x are the same as A_x, and $H_x^{(i,j,k)}$ is offset to $H_x(i, j+\frac{DY}{2}, k+\frac{DZ}{2})$ as shown in Fig. 1. The equation for the components of the magnetic and electric fields are, respectively,

$$\left.\begin{aligned} \mu H_x^{(i,j,k)} &= \frac{A_z^{(i,j+1,k)}-A_z^{(i,j,k)}}{DY} - \frac{A_y^{(i,j,k+1)}-A_y^{(i,j,k)}}{DZ} \\ \mu H_y^{(i,j,k)} &= \frac{A_x^{(i,j,k+1)}-A_x^{(ij,k)}}{DZ} - \frac{A_z^{(i+1,j,k)}-A_z^{(ij,k)}}{DX} \\ \mu H_z^{(i,j,k)} &= \frac{A_y^{(i+1,j,k)}-A_y^{(i,j,k)}}{DX} - \frac{A_x^{(i,j+1,k)}-A_x^{(i,j,k)}}{DY} \end{aligned}\right\} \tag{13}$$

$$\left.\begin{aligned} E_x^{(i,j,k)} &= -j\omega A_x^{(i,j,k)} - \frac{\Phi^{(i+1,j,k)}-\Phi^{i,j,k)}}{DX} \\ E_y^{(i,j,k)} &= -j\omega A_y^{(i,j,k)} - \frac{\Phi^{(i,j+1,k)}-\Phi^{(i,j,k)}}{DX} \\ E_z^{(i,j,k)} &= -j\omega A_z^{(i,j,k)} - \frac{\Phi^{(i,j,k+1)}-\Phi^{(i,j,k)}}{DZ} \end{aligned}\right\} \tag{14}$$

where

$$\begin{aligned} \Phi^{(i,j,k)} &= -\frac{1}{j\omega\mu\varepsilon} \\ &\cdot\left[\frac{A_x^{(i,j,k)}-A_x^{(i-1,j,k)}}{DX}+\frac{A_y^{(i,j,k)}-A_y^{(i,j-1,k)}}{DY}\right. \\ &\left.+\frac{A_z^{(i,j,k)}-A_z^{(i,j,k-1)}}{DZ}\right]. \end{aligned} \tag{15}$$

B. Equation on Dielectric Interface

Solutions of Maxwell's equations written in terms of vector and scalar potentials are only valid in homogeneous media. Equations on the interface are obtained from the continuity conditions of (7)–(9). The continuity of the scalar potential at the interface of Fig. 2 is obtained by equating the scalar potential just above the interface

$$\begin{aligned} &\Phi(y=0^+) \\ &= \frac{-1}{j\omega\mu\varepsilon_0}\left[\frac{A_x^{(0,0,0)}-A_x^{(1,0,0)}}{DX}+\frac{A_y^{(0,0,0)}-A_y^{(0,0,-1)}}{DZ}\right. \\ &\left.+\frac{2\big(A_z^{(0,0,0)}-A_z(y=0)\big)}{DY}\right] \end{aligned} \tag{16}$$

and that just below the interface

$$\begin{aligned} &\Phi(y=0^-) \\ &= \frac{-1}{j\omega\mu\varepsilon_R}\left[\frac{A_x^{(0,0,0)}-A_x^{(1,0,0)}}{DX}+\frac{A_z^{(0,0,0)}-A_z^{(0,0,-1)}}{DZ}\right. \\ &\left.+\frac{2(A_y(y=0)-A_y^{(0,-1,0)})}{DY}\right] \end{aligned} \tag{17}$$

in order to solve for $A_y\,(y=0)$. Then

$$\begin{aligned} \Phi^{(0,0,0)} &= \frac{-2}{j\omega\mu(\varepsilon_0+\varepsilon_R)} \\ &\cdot\left[\frac{A_x^{(0,0,0)}-A_x^{(-1,0,0)}}{DX}+\frac{A_z^{(0,0,0)}-A_z^{(0,0,-1)}}{DZ}\right. \\ &\left.+\frac{A_y^{(0,0,0)}-A_y^{(0,-1,0)}}{DY}\right] \end{aligned} \tag{18}$$

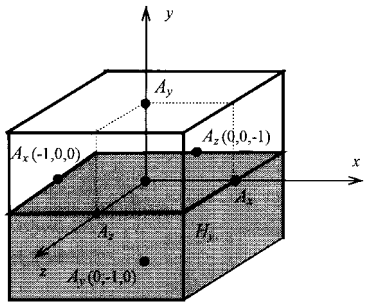

Fig. 2. Values used to find scalar potential on an interface.

which is equivalent to using the average value of the permittivity at the interface. Since this microstrip is parallel to the xz-plane, it is prudent to place the metal surface at a layer where the nodes of A_x and A_z are located. The node locations of A_x, A_z, and the metal boundaries, are shown in Fig. 3, where the 0's indication the location of Φ. The node distribution on the layer at $DY/2$ above or below the metal layer is shown in Fig. 4, where the 0's are for the magnetic scalar potentials if the magnetic current or slot excitation are used. The equation on the metal surface is then

$$\begin{aligned} E_x^{(0,0,0)} &= -j\omega A_x - \frac{\partial \Phi}{\partial x} \\ &= -j\omega A_x^{(0,0,0)} + \frac{(\Phi^{(0,0,0)} - \Phi^{(0,0,1)})}{DX} \\ &= -j\omega A_x^{(0,0,0)} + \frac{2}{j\omega\mu(\varepsilon_0 + \varepsilon_R)} \\ &\quad \cdot \left\{ \left[\frac{A_x^{(1,0,0)} + A_x^{(-1,0,0)} - 2A_x^{(0,0,0)}}{DX \cdot DX} \right] \right. \\ &\quad + \left[\frac{A_z^{(1,0,0)} + A_z^{(0,0,-1)} - A_z^{(1,0,-1)} - A_z^{(0,0,0)}}{DX \cdot DZ} \right] \\ &\quad \left. + \left[\frac{A_y^{(0,-1,0)} + A_y^{(1,0,0)} - A_y^{(1,-1,0)} - A_y^{(0,0,0)}}{DX \cdot DY} \right] \right\} \\ &= 0 \end{aligned} \tag{19}$$

$$\begin{aligned} E_z^{(0,0,0)} &= -j\omega A_z - \frac{\partial \Phi}{\partial z} \\ &= -j\omega A_z^{(0,0,0)} + \frac{2}{j\omega\mu(\varepsilon_0 - \varepsilon_R)} \\ &\quad \cdot \left\{ \left[\frac{A_z^{(0,0,1)} + A_z^{(0,0,-1)} - 2A_z^{(0,0,0)}}{DZ \cdot DZ} \right] \right. \\ &\quad + \left[\frac{A_x^{(1,0,0)} + A_x^{(-1,0,0)} - A_x^{(-1,0,1)} - A_x^{(0,0,0)}}{DX \cdot DZ} \right] \\ &\quad \left. + \left[\frac{A_y^{(0,-1,0)} + A_y^{(0,0,1)} - A_y^{(0,-1,1)} - A_y^{(0,0,0)}}{DZ \cdot DY} \right] \right\} \\ &= 0. \end{aligned} \tag{20}$$

The metal edges and corners are placed in the meshed region in Fig. 3, where the singularities of the edge and corner electric fields are nicely avoided.

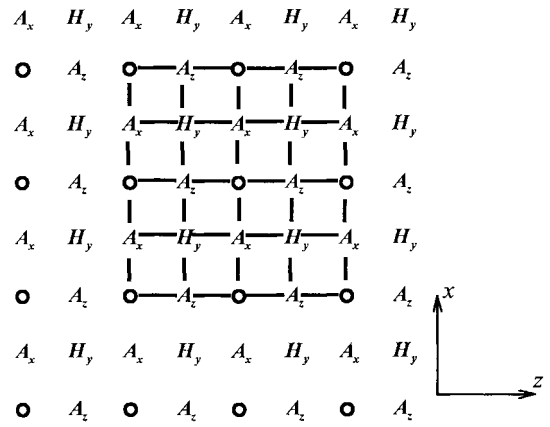

Fig. 3. Locations of the vector potential components in relation to metal boundary.

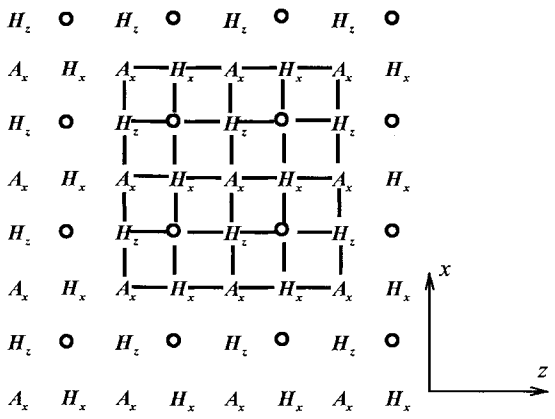

Fig. 4. Locations of the vector potential components one half division above the metal surface.

The continuity of the tangential magnetic field at the interface is obtained by the integral

$$\mu \oint_C \bar{H} \cdot \overline{dl} - j\omega \int_s \bar{D} \cdot \overline{ds} = 0. \tag{21}$$

Let the loop integral be on the xy- and zy-plane, respectively, to obtain

$$\begin{aligned} &\left[\frac{2}{DX^2} + \frac{2}{DY^2} + \frac{2}{DZ^2} - k_{\text{ave}}^2 \right] A_z^{(0,0,0)} \\ &\quad - \left\{ \frac{A_z^{(1,0,0)} + A_z^{(-1,0,0)}}{DX^2} + \frac{A_x^{(0,1,0)} + A_x^{(0,-1,0)}}{DY^2} \right. \\ &\quad \left. + \frac{A_z^{(0,0,1)} + A_z^{(0,0,-1)}}{DZ^2} \right\} = 0 \end{aligned} \tag{22}$$

and

$$\begin{aligned} &\left(\frac{2}{DX^2} + \frac{2}{DY^2} + \frac{2}{DZ^2} - k_{\text{ave}}^2 \right) A_x^{(0,0,0)} \\ &\quad - \left\{ \frac{A_x^{(1,0,0)} - A_x^{(-1,0,0)}}{DX^2} + \frac{A_x^{(0,1,0)} + A_x^{(0,-1,0)}}{DY^2} \right. \\ &\quad \left. + \frac{A_x^{(0,0,1)} + A_x^{(0,0,-1)}}{DZ^2} \right\} = 0 \end{aligned} \tag{23}$$

where

$$k_{\text{ave}}^2 = \omega\mu\frac{\varepsilon_0 - \varepsilon_R}{2}. \tag{24}$$

An interesting case is the equation for A_y just above and below the interface. Even though they are interior nodes, they are only a half discretization away from the interface, and the central FD equation would require a node in the other medium. The integral of (21) in the xz-plane just above and below the interface gives the following formulas, respectively,

$$\left[-k_0^2 + \frac{2}{DX^2} + \frac{2}{DZ^2} + \frac{2}{DY^2}\left(1 + \frac{2\varepsilon_0}{\varepsilon_R + \varepsilon_0}\right)\right]A_y^{(0,0,0)} - \left[\frac{A_y^{(0,0,1)} + A_y^{(1,0,0)}}{DZ^2} + \frac{A_y^{(1,0,0)} + A_y^{(-1,0,0)}}{DX^2} + \frac{A_y^{(0,1,0)} + \frac{2\varepsilon_0}{\varepsilon_0+\varepsilon_R}A_y^{(0,-1,0)}}{DY^2}\right] + \left(1 - \frac{2\varepsilon_0}{\varepsilon_0 + \varepsilon_R}\right) \cdot \left(\frac{A_x^{(-1,0,0)} - A_x^{(0,0,0)}}{DX \cdot DY} + \frac{A_z^{(0,0,-1)} - A_z^{(0,0,0)}}{DZ \cdot DY}\right) = 0 \tag{25}$$

and

$$\left[-k_0^2\left(\frac{\varepsilon_R}{\varepsilon_0}\right) + \frac{2}{DX^2} + \frac{2}{DZ^2} + \frac{2}{DY^2}\left(1 + \frac{2\varepsilon_0}{\varepsilon_R + \varepsilon_0}\right)\right]A_y^{(0,0,0)} - \left(\frac{A_y^{(0,0,1)} + A_y^{(0,0,-1)}}{DZ^2} + \frac{A_y^{(1,0,0)} + A_y^{(-1,0,0)}}{DX^2} + \frac{A_y^{(0,-1,0)} + \frac{2\varepsilon_R}{\varepsilon_0+\varepsilon_R}A_y^{(0,1,0)}}{DY^2}\right) + \left(1 - \frac{2\varepsilon_0}{\varepsilon_0 + \varepsilon_R}\right) \cdot \left(\frac{A_x^{(0,1,0)} - A_x^{(-1,1,0)}}{DX \cdot DY} + \frac{A_z^{(0,1,0)} - A_z^{(0,1,-1)}}{DZ \cdot DY}\right) = 0. \tag{26}$$

These pseudo-interior equations are functions of the medium of the other side.

III. Implementation of the MEI Method

A. Linear Equations

The MEI method to terminate the mesh, or to write local linear equations at the mesh boundary is described. Fig. 5 shows three types of node configuration for a cubic mesh enclosure. Therefore, the mesh boundary equations are

$$\sum_{i=0}^{N} a_i A_\alpha(\bar{r}_i) = 0, \qquad \alpha = x, y, \text{ or } z \tag{27}$$

where $N = 2, 3, 4$ for corner, edge, and surface nodes, respectively. Note that the mesh boundary equations are derived for each wave equation of the components of $\bar{A}$, so there is no coupling between them in (27). There should be a different set of a_i for every A_α.

The measuring functions are

$$\bar{A}^{(k)}(\bar{r}) = \int_s \underline{\underline{G}}(\bar{r}/x', z') \cdot \vec{J}_k(x', z')ds'. \tag{28}$$

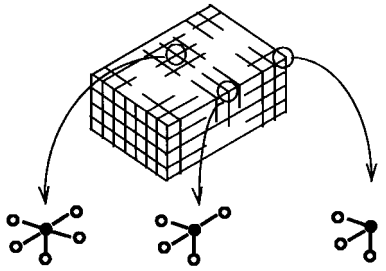

Fig. 5. Geometry of boundary nodes of a 3-D mesh.

The $\underline{\underline{G}}(\bar{r}/x', z')$ is the dyadic Green's function for the ground plane with dielectric substrate, s is the surface of the microstrip or antenna, and $\bar{J}_k$ is the metron on s.

For each $k \in \{1, 2, \cdots, M\}$, the values of $\bar{A}^{(k)}$ may be inserted into (27) generating a linear system which may be used to find the MEI coefficients a_i. As in the static case described earlier, the value is arbitrary, set to $a_0 = -1$

$$a_1^{(\alpha)}A_\alpha^{(k)}(\bar{r}_1) + a_2^{(\alpha)}A_\alpha^{(k)}(\bar{r}_2) + \cdots + a_N^{(\alpha)}a_\alpha^{(k)}(\bar{r}_N) = A_\alpha^{(k)}(\bar{r}_0), \qquad k \in \{1, 2, \cdots, M\},\ M \geq N. \tag{29}$$

This is done for each node on the mesh surface, edge or corner, where the FD equations fail.

B. The Metrons

In the case of a 2-D problem the choice of a metron set, though arbitrary, is quite simple, such as the lowest order terms of any orthogonal set of functions. In a 3-D case, where a 2-D surface may assume quite complicated shapes, an intuitive selection of metrons may not be available. To relieve the code developer the burden of choosing particular metron sets, the authors have decided to use Hertzian dipoles at the nodes as metrons. One a-directed Hertzian dipole is placed at one node location of A_α as a metron for $A_\alpha(\bar{r})$. Therefore, we shall have M metrons, and M is the number of node points of A_α on the metal surface where $M \gg N$. A least square fit is used to find the N coefficients in (27). Surprisingly, all M equations are very nearly satisfied. Maximum residues in (27) are about 1% for every node in the mesh and for every measuring function. The least-square procedure is very much like an integration process in (28). The rule is that every node point of A_α on the metal should be included.

C. The Green's Functions

The Green's function in (28) is a dyadic of the form

$$\underline{\underline{G}} = \begin{bmatrix} A_x^x & O & O \\ A_y^x & A_y^y & A_y^z \\ O & O & A_z^z \end{bmatrix}. \tag{30}$$

The components in (30) are given in terms of Sommerfeld's integrals. They are the solutions to the Helmholtz equation in regions of a grounded planar dielectric substrate shown in Fig. 6. An excellent reference to those is [18]. The superscript in (30) denotes the direction of the source and the subscript denotes that of the potential. The integrals are shown in (31)–(33) at the bottom of the following page,

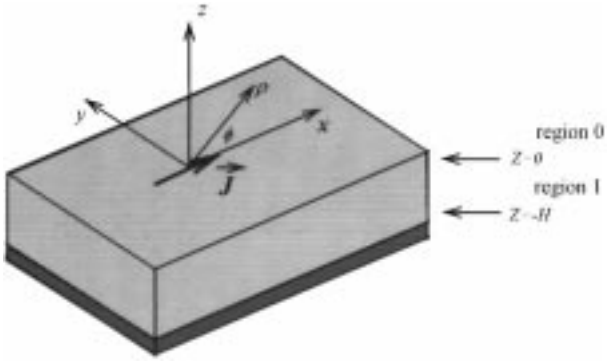

Fig. 6. Geometry for finding the Sommerfeld integrals of a grounded dielectric substrate.

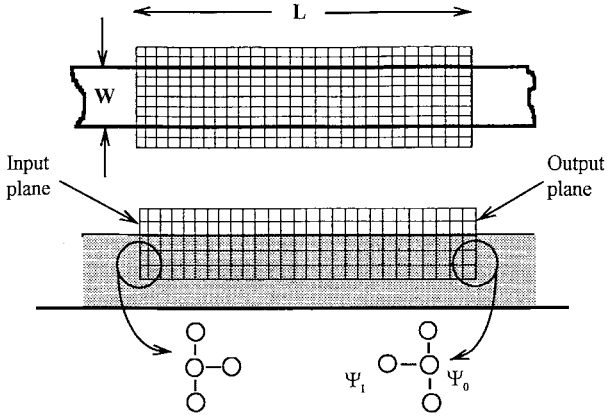

Fig. 7. Mesh geometry of an infinite line using MEI.

where $D_{\mathrm{TE}} = u_1 \cosh(u_1 H) + u_0 \sinh(u_1 H)$, and $D_{\mathrm{TM}} = \varepsilon_1 u_0 \cosh(u_1 H) + \varepsilon_0 u_1 \sinh(u_1 H)$. The symmetry of the media gives the following relations:

$$\left.\begin{aligned} A_x^x(x,y,z) &= A_z^z(-z,y,x) \\ A_y^x(x,y,z) &= A_y^z(-z,y,x) \end{aligned}\right\}. \tag{34}$$

The integrations of the Green's functions are time consuming because the integrands are slowly decaying oscillating functions. Techniques for performing such integrations are outlined in [18].

IV. Numerical Results

Using the above procedures, the FD equations are developed and truncated specifically for planar-microstrip-type problems. All one needs to do is to use a sparse matrix subroutine to solve for the vector potentials, from which the fields and induced current densities can be obtained. The advantage offered by the MEI procedure is its capability to truncate the mesh very close to the object surface—in this cases, the microstrip itself. In the horizontal direction the mesh is terminated only two discretization steps away from the edges of the metal strip. In the vertical direction, the mesh is terminated two discretization steps above the strip and three discretization steps below the strip.

A. Infinite Structures

A microstrip line extending to infinity is a basic problem for numerical computation because it will tell us how well the method can model transmission structures. The geometry for a continuous line is shown in Fig. 7. The FD equation inside the mesh, and the MEI equations at most of the edges of the mesh, have been derived in the previous section. However, something else should be done at the input and output planes. Since we are looking for a wave which propagates with a z-dependence of the form $\exp(-j\beta z)$, this condition can be enforced at the output plane, by writing

$$\psi_0 = \exp(-j\beta DZ) \cdot \psi_1. \tag{35}$$

The input plane now forms the excitation for the problem. An iterative method may be used to derive the excitation. The first step is to specify $A_z = 1$ on the metal and zero off the metal at the input plane. The system of equations is solved. The values calculated at the output plane may be used as the new excitation values at the input plane and the calculation is repeated. Because the higher order modes, which are excited, decay in the z-direction, the solution should stabilize to a dominant mode after a few iterations, which it does. Note that the MEI coefficients, or all the elements of the matrix, remain unchanged at each iteration.

Another issue in modeling an infinite line is the effect of the presence of the metrons outside the mesh. Metrons are placed outside of the mesh where the effect is seen to be negligible to compare to the effect of closer current effects. In other words, the metal effect is deemed to continue to some distance away

$$A_z^z = \begin{cases} \dfrac{1}{2\pi}\displaystyle\int_0^\infty \frac{\sinh(u_1(y+H))}{D_{\mathrm{TE}}} J_0(k_\rho \rho)\, dk_\rho, & y \le 0 \\ \dfrac{1}{2\pi}\displaystyle\int_0^\infty \frac{\sinh[(u_1 H)]\exp[(-u_0 y)]}{D_{\mathrm{TE}}} J_0(k_\rho \rho) k_\rho\, dk_\rho, & y \ge 0 \end{cases} \tag{31}$$

$$A_z^y = \begin{cases} -\dfrac{\cos\phi}{2\pi}\displaystyle\int_0^\infty \frac{(\varepsilon_1 - \varepsilon_0)\sinh[(u_1 H)]\cosh[(u_1(y+H))]}{D_{\mathrm{TE}} + D_{\mathrm{TM}}} J_1(k_\rho \rho) k_\rho^2\, dk_\rho, & y \le 0 \\ -\dfrac{\cos\phi}{2\pi}\displaystyle\int_0^\infty \frac{(\varepsilon_1 - \varepsilon_0)\sinh(u_1 H)\cosh(u_1 H)\exp[(-u_0 y)]}{D_{\mathrm{TE}} D_{\mathrm{TM}}} J_1(k_\rho \rho) k_\rho^2\, dk_\rho, & y \ge 0 \end{cases} \tag{32}$$

$$A_y^y = \begin{cases} \dfrac{1}{2\pi}\displaystyle\int_0^\infty \frac{-2\lambda \cosh u_0(y+H)}{D_{\mathrm{TM}}} J_0(k_\rho \rho) k_\rho\, dk_\rho, & y \le 0 \\ \dfrac{1}{2\pi}\displaystyle\int_0^\infty \frac{\lambda}{\omega_0} \frac{(u_0 n^2 \cosh(\mu_E H) - u_1 \sinh(\mu_E H))\exp[u_0 y]}{D_{\mathrm{TM}}} J_0(k_\rho \rho) k_\rho\, dk_\rho, & y \ge 0 \end{cases} \tag{33}$$

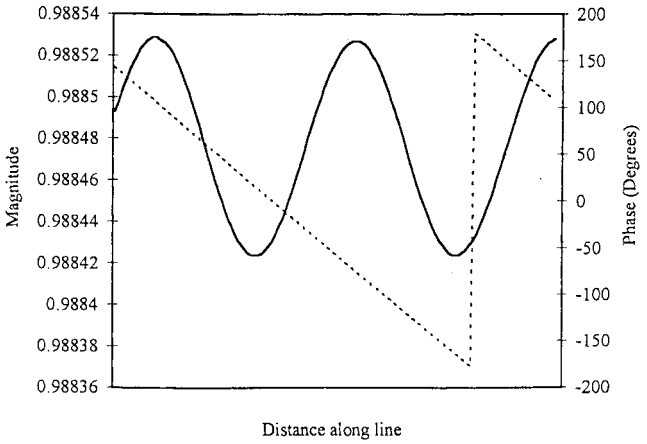

Fig. 8. Current along an infinite suspended strip. $H = 1$ mm, frequency $= 12$ GHz.

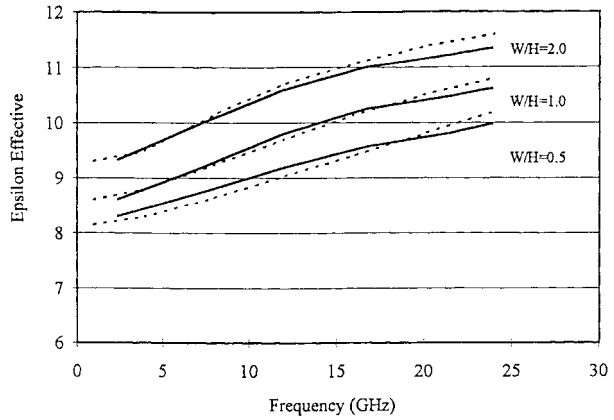

Fig. 9. Effective dielectric constant for microstrip lines. Relative dielectric permittivity is 12.9, and substrate thickness is 1 mm, $\varepsilon_{\text{eff}} = (\beta/k_0)^2$. The dotted line is from [20].

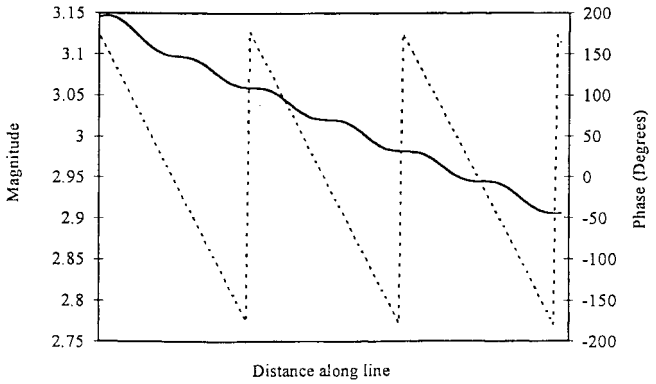

Fig. 10. Current along an infinite microstrip line. Frequency is 12 GHz, substrate is the same as in Fig. 17, and $w/H = 1.0$.

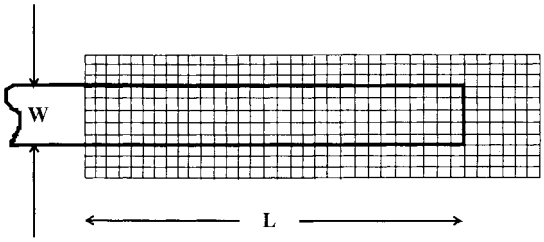

Fig. 11. Mesh geometry of an open-end microstrip. $W = 6h$, $L = 50h$, $H = 6.5h$, $0.01 \leq k_0 h < 0.06$, where h is the mesh spacing (L not to scale).

from each side of the mesh, and Hertzian dipole metrons are place at each node on the metal. Then, the MEI coefficients are found by a least-square-fitting method. Through numerical experimentation, it has been found that placing metrons out to a distance equal to about $15H$, where H is the thickness of the substrate, produces good results. The magnitude and phase of the total longitudinal current along a suspended strip is shown in Fig. 8. A tiny standing wave is seen, representing the size of the error in the calculation.

For a microstrip where the substrate is not air, the propagation constant is unknown. However, it may be found by the same iterative process used to find the excitation values on the input plane. First, a starting β value may be found from the quasi-static approximation, and the initial excitation of A_z as used earlier. Then, after each solution, a new propagation constant is calculated from the slope of the phase along the transmission line. The new value of β along with the new excitation values are inserted into the problem and resolved. The process is repeated until the propagation approaches a unimodal form

$$A(x, y, z) = A(x, y) \exp(-j\beta z). \tag{36}$$

The MEI coefficients stay the same in each iteration, but the equations at the output plane (35) do change because of the changing β. In addition, it is found that the best results are obtained when the mesh is extended all the way to the ground plane.

Results using this approach are shown in Fig. 9. The longitudinal current densities, magnitude, and phase of the same line of Fig. 7 with a dielectric layer of $\varepsilon_r = 12.9$ at 12 GHz are shown in Fig. 10. For this inhomogeneous case, the solution is not quite as accurate as in the homogeneous case. The magnitude of the current decreases as it propagates, in other words, the propagation constant has a small imaginary part. This error appears due to numerical inaccuracies in the FD and MEI equations. It becomes smaller as the mesh size is reduced. The same numerical phenomenon has been observed when the finite-difference time-domain (FDTD) method is used [21]. Actually using this 3-D approach to calculate what is, in fact, a 2-D problem is overkill. A more common method to solve for the propagation constant for an infinite line is the spectral-domain method [22]. The 3-D approach is used to test how well the MEI method models infinite structures.

B. Microstrip Discontinuities

Open End: The simplest microwave discontinuity is the open end, shown in Fig. 11. The excitation used at the input plane is the potential of an infinite line. Since higher order modes are excited at the open end, the input plane should be placed some distance away from the open end. Experience indicates that a distance of about $8H$ works well.

In order to extract the reflection coefficient, the current on the line must be decomposed into the sum of a forward and a reflected wave

$$J(Z) = A^+ \exp(-\Gamma Z) - A^- \exp(\Gamma Z). \tag{37}$$

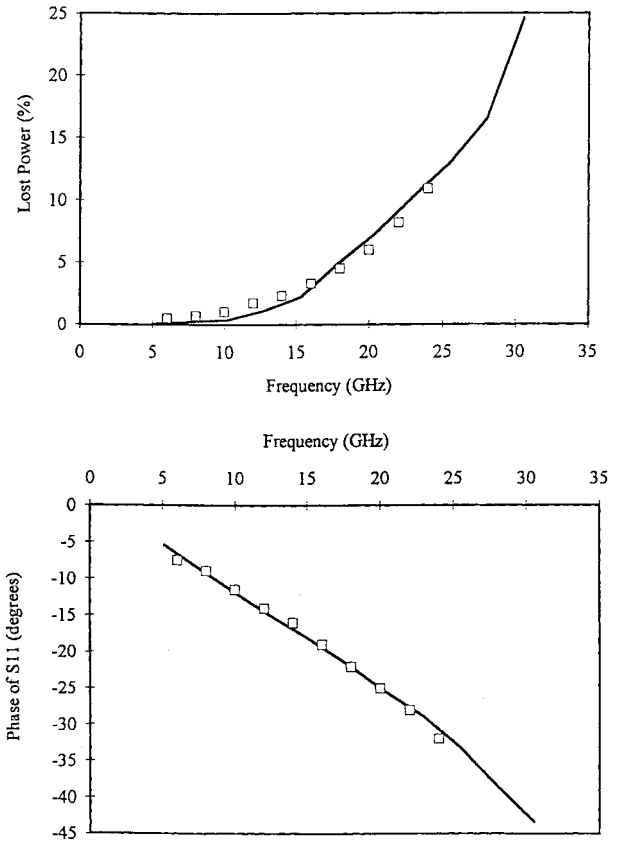

Fig. 12. Lost power and S_{11} of the microstrip open end. The relative permittivity is 9.9, substrate thickness is 0.06 cm, strip width is 0.06 cm. The solid lines are results using the MEI, and the points are from [23].

The value of Γ is found from the infinite line problem with the same mesh size. The magnitude of A^+ and A^- may be found by equating the calculated current on the line to the form of (37). The reflection coefficient is

$$S_{11} = A^-/A^+. \tag{38}$$

Results for the reflection coefficient are given in Fig. 12. The top view of the mesh is shown in Fig. 11 except that L is not in scale. The mesh extends $2h$ above and $4h$ below the interface. The calculated results of Fig. 12 agree well with those of [30].

Microstrip Bend: The geometry and mesh of a microstrip bend is shown in Fig. 13. The mesh is extended to $2h$ above and $3h$ below the interface. Metron currents are placed up to a distance of 100 mesh units from the bend. Good agreement of the S-parameters with earlier calculations [30] is shown in Fig. 14. The power radiated is found from

$$P_{\text{rad}} = 1 - |S_{11}|^2 - |S_{12}|^2. \tag{39}$$

The actual magnitude of the current density over the strip is shown in Fig. 15. The standing wave at the input side is clearly seen, as is the characteristic profile of the current densities traversing the microstrip.

Microstrip Stub: Another example in the literature is the analysis of a microstrip stub, shown in Fig. 16. The mesh is shown in scale except for the length along the strip. The mesh actually extends 50 points in each direction. In the vertical direction, the mesh extends $2h$ above and $3h$ below the interface. The current densities on the stub are shown in Fig. 17. The results contain all the features one would expect from the current densities in a microstrip, such as high-longitudinal-current densities along the metal edge, standing wave on the input side of the strip, small transverse current, etc. Fig. 18 shows the S-parameters and total scattered power.

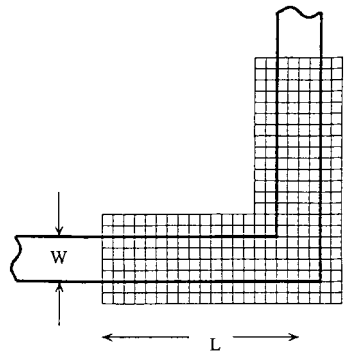

Fig. 13. Mesh geometry of a microstrip bend. $W = 4h$, $L = 50h$, $H = 4.5h$, $0.01 \leq k_0 h \leq 0.08$, where h is the mesh spacing.

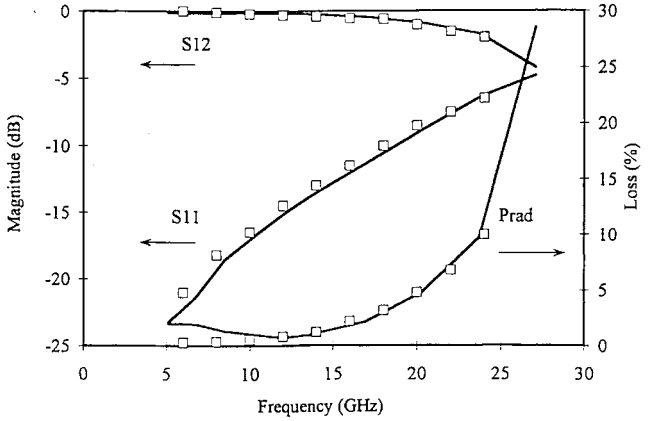

Fig. 14. S-parameters of the microstrip bend. Relative permittivity of substrate is 9.9. Strip width and substrate thickness both are 0.06 cm. Solid line is by MEI, points are from [23].

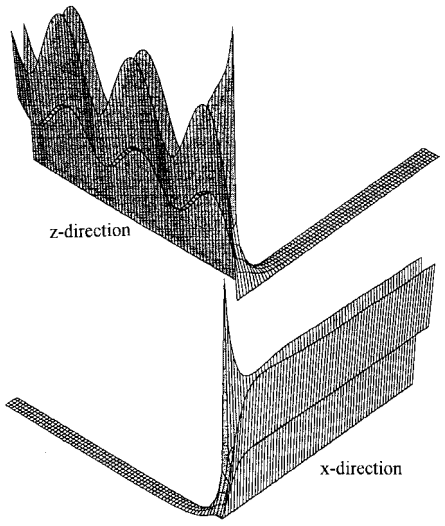

Fig. 15. Current densities on the microstrip bend of Fig. 13. The frequency is 17 GHz.

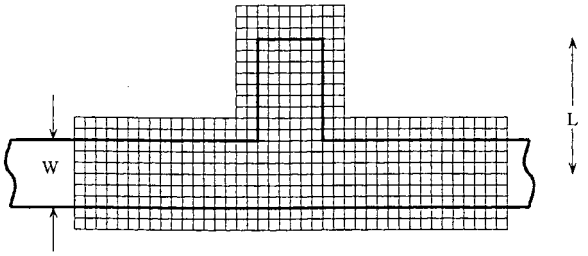

Fig. 16. Mesh geometry of a microstrip stub. Mesh is shown to scale, except for the length along the input and output. The mesh actually extends 50 points in each direction.

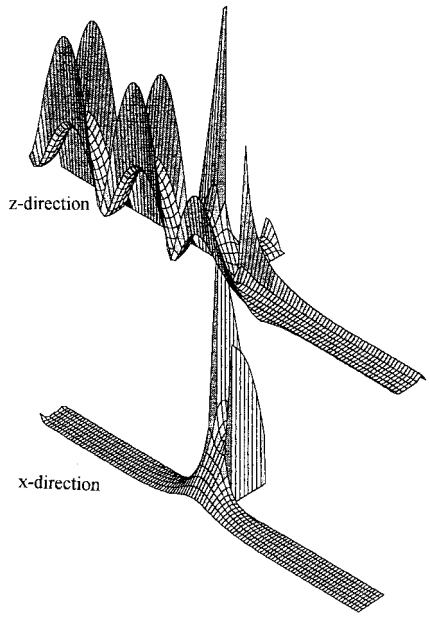

Fig. 17. Current on a stub discontinuity. Frequency is 10.25 GHz.

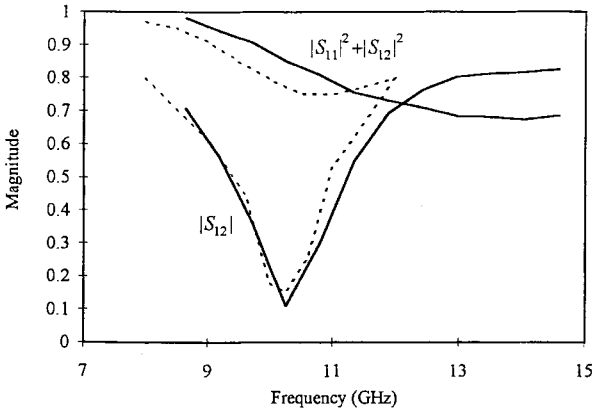

Fig. 18. S-parameters of the microstrip stub of Fig. 16. $\varepsilon_R = 10.65$, $L = 2.8$ mm, $W = 1.4$ mm, $H = 1.27$ mm. Dashed line is from [24].

One less the scattered power should be the power radiated. The comparison of this calculation and that of the prior work by Jackson[1] [24] is shown in Fig. 18. Results similar to Jackson's were reported in [25] using the MoM.

[1]Despite the title of the paper, the calculations in Jackson's paper are done by the MoM.

V. Conclusion

The authors have shown that the MEI method can be applied to 3-D planar microstrip structures. This method has successfully truncated the FD mesh very close to the microstrip surface without disturbing the sparsity of the matrix so that the size of the problem is reduced to within the limits of a personal computer. This paper is just a demonstration of the validity of the MEI method. The real value of the MEI method is its potential of tackling large problems such as filters, couplers, and antenna arrays. Improvements of the existing codes regarding more complex geometry and speeding up of the Sommerfeld's integrals have to be done before one can economically solve large problems.

The MEI method has a big advantage in its simplicity. It actually simplifies the mesh generation for FD/FE problems because the mesh does not need to extend very far from the body surface. In this work, a variety of microstrip discontinuity problems with the same code have been analyzed. Little setup time is needed to switch from one to the other. All that must be done to specify the problem is to describe the location of the metal nodes and the form of excitation.

References

[1] K. K. Mei, R. Pous, Z. Chen, Y. Liu, and M. Prouty, "The measured equation of invariance—A new concept in field computation," *IEEE Trans. Antennas Propagat.*, vol. 42, pp. 320–328, Mar. 1994.

[2] K. K. Mei, R. Pous, Z. Chen, and Y. Liu, "Measured equation of invariance—A new concept in field computation," in *IEEE AP-S Int. Sym. Dig.*, Chicago, IL, July 1992, pp. 2047–2050.

[3] J. Jevtic and R. Lee, "An analysis of the measured equation of invariance," in *URSI Radio Sci. Meeting*, Ann Arbor, MI, June 1993, p. 256.

[4] J. L. Young, J. B. Schneider, and R. G. Olsen, "Theoretical aspect on the measured equation of invariance," in *URSI Radio Sci. Meeting*, Ann Arbor, MI, June 1993, p. 257.

[5] D. B. Wright and A. C. Cangellaris, "MEI-based truncation conditions for the finite element modeling of EM scattering by two-dimensional penetrable objects," in *URSI Radio Sci. Meeting*, Ann Arbor, MI, June 1993, p. 258.

[6] Y. Li, Z. J. Cendes, and X. Yuan, "A modified MEI method for solving scattering problem with the finite element method," in *IEEE AP-S Int. Symp.*, Ann Arbor, MI, June 1993, pp. 284–287.

[7] R. Pous, M. Prouty, and K. K. Mei, "Application of the measured equation of invariance to radiation and scattering by flat surfaces," in *IEEE AP-S Int. Sym. Dig.*, Ann. Arbor, MI, June 1993, pp. 540–543.

[8] R. Gordon, R. Mittra, A. Glisson, and E. Michielssen, "An efficient numerical boundary condition for the truncation of finite meshes for analysis of electromagnetic scattering by complex bodies," in *IEEE AP-S Int. Symp., Dig.*, Ann Arbor, MI, June 1993, pp. 288–291.

[9] K. K. Mei, R. Pous, M. Prouty, and Y. Liu, "Further insight into MEI method," in *IEEE AP-S Symp. Dig.*, Ann Arbor, MI, June 1993, pp. 544–546.

[10] M. Prouty, S. Schwarz, R. Pous, K. K. Mei, and Y. Liu, "Microstrip discontinuities using the measured equation of invariance," in *IEEE MTT-S Symp. Dig.*, San Diego, CA, May 1994, pp. 595–598.

[11] J. Jevtics and R. Lee, "A theoretical and numerical analysis of the measured equation of invariance," *IEEE Trans. Antennas Propagat.*, vol. 42, pp. 1097–1105, Aug. 1994.

[12] K. K. Mei and Y. Liu, "Comments on 'A theoretical and numerical analysis of the measured equation of invariance,'" *IEEE Trans. Antennas Propagat.*, vol. 43, pp. 1168–1170, Oct. 1995.

[13] R. Pous, "The measured equation of invariance: A new concept in field computation," Ph.D. dissertation, EECS Dept., Univ. of California, Berkeley, 1992.

[14] M. Prouty, S. Schwarz, K. K. Mei, R. Pous, and Y. Liu, "A new approach to quasi-static analysis with application to microstrip," *IEEE Microwave Guided Wave Lett.*, vol. 3, pp. 302–304, Sept. 1993.

[15] M. Prouty, R. Pous, K. K. Mei, and S. Schwarz, "Application of the measured equation of invariance to transmission lines and discontinu-

ities," in *IEEE AP-S, Int. Symp. Dig.*, Ann Arbor, MI, June 1993, pp. 280–283.
[16] M. Prouty, "Application of the measured equation of invariance to planar microstrip structures," Ph.D dissertation, EECS Dept., Univ. of California, Berkeley, 1994.
[17] K. S. Yee, "Numerical solution of initial boundary value problems involving Maxwell's equation in isotropic media," *IEEE Trans. Antennas Propagat.*, vol. 14, pp. 302–307, May 1966.
[18] J. R. Mosig and F. E. Gardiol, "Adynamic radiation model for microstrip structure," in *Advances in Electronics and Electronic Physics*. New York: Academic Press, 1982, vol. 59, pp. 139–237.
[19] N. K. Uzunoglu, N. G. Alexopolous, and J. G. Fikioris, "Radiation properties of microstrip dipoles," *IEEE Trans. Antennas Propagat.*, vol. 27, pp. 853–858, Nov. 1979.
[20] R. E. Collin, *Field Theory of Guided Waves*, 2nd ed. Piscataway, NJ: IEEE Press, 1992.
[21] X. Zhang, J. Fang, K. K. Mei, and Y. Liu, "Calculation of the dispersive characteristics of microstrips by the time-domain finite difference method," *IEEE Trans. Microwave Theory Tech.*, vol. 36, pp. 263–267, Feb. 1988.
[22] D. Mirshekar-Syahkal, *Spectrum Domain Method for Microwave Integrated Circuits*. Taunton, Sommerset, U.K.: Research Studies Press, 1990.
[23] T. Horng, W. E. Mckinzie, and N. G. Alexopolous, "Full-wave spectral-domain analysis of compensation of microstrip discontinuities, using triangular subdomain functions," *IEEE Trans. Microwave Theory Tech.*, vol. 40, pp. 2137–2147, Dec. 1992.
[24] R. W. Jackson, "Full-wave, finite element analysis of irregular microstrip discontinuities," *IEEE Trans. Microwave Theory Tech.*, vol. 37, pp. 81–89, Jan. 1989.
[25] W. P. Harokopus Jr. and P. B. Katehi, "Characterization of microstrip discontinuities on multilayer dielectric substrates including radiation losses," *IEEE Trans. Microwave Theory Tech.*, vol. 37, pp. 2058–2065, Dec. 1989.

Mark D. Prouty (M'88) received the B.A. degree in physics from the University of Chicago, Chicago, IL, in 1982, and M.S. and Ph.D. degrees from the University of California, Berkeley, in 1984 and 1994, respectively.

He worked in circuit design for Schlumberger Well Services and Fairchild Weston Systems from 1984 through 1989, designing downhole electromagnetic instrumentation and high-speed video cameras. In 1994 he worked as a management consultant for McKinsey and Company. He is currently Vice President of Engineering at Geometrics, Inc., Sunnyvale, CA, having responsibility for the development of new geophysical instruments.

Kenneth K. Mei (S'61–M'63–SM'76–F'79) received the B.S.E.E., M.S. and Ph.D. degrees in electrical engineering from the University of Wisconsin, Madison, in 1959, 1960, and 1962, respectively.

He joined the faculty of the Department of Electrical Engineering and Computer Sciences, University of California, Berkeley, in 1962, and since 1972 has been a Professor there. In 1992, he also became a Professor of Buddhist Study at Berkeley. He is now an Emeritus Professor of the University of California. Since 1994 he has been a Professor in the Department of Electronic Engineering, the City University of Hong Kong, Kowloon. He began his research in electromagnetics in the area of computation, which includes the method of moments, finite-element/finite-difference, hybrid methods, time-domain methods, and most recently the measured equation of invariance.

Dr. Mei is a member URSI/USNC. He received the Best Paper Award in 1967 and Honorable Mention of the Best Paper Award in 1974 from the IEEE Antennas and Propagation Society.

Steven E. Schwarz (SM'71–F'92) was born in Los Angeles in 1939. He received the B.S. degree in physics from the California Institute of Technology, Pasadena, the A.M. degree in physics from Harvard University, Cambridge, MA, and the Ph.D. degree in electrical engineering from California Polytechnic State University, San Luis Obispo, in 1959, 1962, and 1964, respectively.

He has held positions with Hughes Research Laboratories, AT&T Bell Laboratories, and IBM Research Laboratories. Since 1964 he has been a member of the Department of Electrical Engineering and Computer Sciences, University of California, Berkeley. His research deals with devices and techniques for planar microwave circuits.

Prof. Schwarz held a Guggenheim fellowship in 1971–1972 and in 1990–1993 occupied the President's Chair in Undergraduate Education at Berkeley.

Rafael Pous (S'89–M'93) was born in Barcelona, Spain, in 1964. He received the Ingeniero degree in telecommunications engineering, and the Licenciado degree in computer science from the Polytechnic University of Catalonia, Barcelona, Spain, in 1988, the M.S. degree in electrical engineering from the University of Massachusetts, Amherst, in 1989, and the Ph.D. degree in electrical engineering from the University of California, Berkeley, in 1992.

In 1993, he joined the telecommunications engineering faculty of the Polytechnic University of Catalonia. His research interests are in the area of computational electromagnetics and applied superconductivity.

Dr. Pous was awarded the Fulbright Scholarship and the Schlumberger Fellowship during his studies.

Yao-wu Liu received the M.S., and Ph.D. degrees from the University of Electronic Science and Technology of China, Chengdu, China, in 1981 and 1984, respectively.

He was a Research Associate with the Department of Electrical Engineering, University of Utah, Salt Lake City, from April to November in 1986, and a Research Scientist with the Department of Electrical Engineering, State University of New York at Binghamton, from May to August in 1993. From December of 1986 to February of 1995, he was a Research Scientist with the Department of Electrical Engineering and Computer Science, University of California at Berkeley. He was also a Microwave and Radio-Frequency Consultant working for several wireless communications companies in the U.S. He joined the Department of Electronic Engineering, City University of Hong Kong, Kowloon, in March 1995, and is now a Research Assistant Professor. His research interests include electromagnetic theory and numerical computational methods (time-domain/finite-difference, finite-element, integral-equation methods, etc.) to solve electromagnetic problems, such as scattering, antennas, microwave circuits, VLSI interconnects, and MCM packagings.